analytical chemistry

Article

Cite This: Anal. Chem. 2019, 91, 5953−5960

pubs.acs.org/ac

Design and Demonstration of Tunable Amplified Sensitivity of AlGaN/GaN High Electron Mobility Transistor (HEMT)-Based Biosensors in Human Serum

Tse-Yu Tai,[†] Anirban Sinha,[†] Indu Sarangadharan,[†] Anil Kumar Pulikkathodi,[†] Shin-Li Wang,[†] Geng-Yen Lee,[∥] Jen-Inn Chyi,[∥] Shu-Chu Shiesh,[⊥] Gwo-Bin Lee,*[,†,‡,§] and Yu-Lin Wang*[,†,‡]

[†]Institute of Nanoengineering and Microsystems, [‡]Department of Power Mechanical Engineering, and [§]Institute of Biomedical Engineering, National Tsing Hua University, Hsinchu 300, Taiwan, R.O.C

[∥]Department of Electrical Engineering, National Central University, Zhongli District, Taoyuan City 320, Taiwan, R.O.C

[⊥]Department of Medical Laboratory Science and Biotechnology, National Cheng Kung University, Tainan City 701, Taiwan, R.O.C

Supporting Information

ABSTRACT: We have developed a swift and simplistic protein immunoassay using aptamer functionalized AlGaN/GaN high electron mobility transistors (HEMTs). The unique design of the sensor facilitates protein detection in a physiological salt environment overcoming charge screening effects, without requiring sample preprocessing. This study reports a tunable and amplified sensitivity of solution-gated electric double layer (EDL) HEMT-based biosensors, which demonstrates significantly enhanced sensitivity by designing a smaller gap between the gate electrode and the detection, and by operating at higher gate voltage. Sensitivity is calculated by quantifying NT-proBNP, a clinical biomarker of heart failure, in buffer and untreated human serum samples. The biosensor depicts elevated sensitivity and high selectivity. Furthermore, detailed investigation of the amplified sensitivity in an increased ionic strength environment is conducted, and it is revealed that a high sensitivity of 80.54 mV/decade protein concentration can be achieved, which is much higher than that of previously reported FET biosensors. This sensor technology demonstrates immense potential in developing surface affinity sensors for clinical diagnostics.

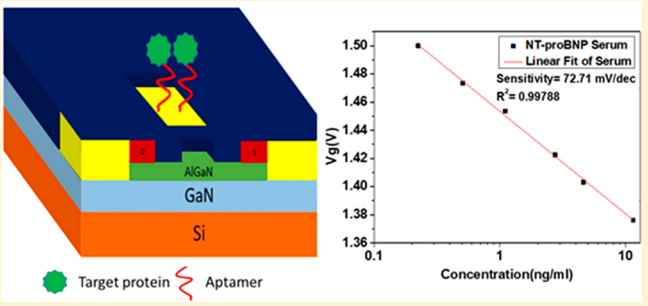

Molecular diagnostics aim to analyze biomarkers such as proteins for early diagnosis of diseases and risk assessment.[1,2] Protein-based biomarkers have been routinely used for the diagnosis of various cardiovascular diseases (CVDs), which contribute to the greatest number of deaths in the world today.[3−5] Among CVDs, heart failure (HF) progresses slowly and results in excessive cost burden in terms of treatment and disease management. HF can be better managed or even prevented if an individual's blood-based protein biomarkers are analyzed, which provides additional risk stratification beyond the conventional disease markers.[5] Brain natriuretic peptides (BNP) have been used in clinical diagnostics for the diagnosis and prognosis of heart failure.[6−8] The amine terminated fragment of the proBNP molecule called NT-proBNP is a relatively more stable natriuretic peptide with a longer half-life in circulation.[9,10] Therefore, NT-proBNP has emerged as an important clinical marker of HF in the recent years.

Current clinical diagnostics for NT-proBNP are mainly optical-based detection methodologies such as electrochemiluminiscence (Roche cobas e 411) and enzyme immunoassay (Biomedica Gruppe). They require the use of sophisticated benchtop instruments, trained laboratory personnel to carry out sample pretreatments, and long turnaround times, because of which these assays can be performed only in clinical settings. Therefore, the present clinical diagnostics are not accessible to people widely and are highly inconvenient, posing problems such as delayed diagnosis and poor prognosis. The drawbacks of current techniques can be overcome by developing point-of-care and home-care tests that assay protein biomarkers in automated fashion while retaining or enhancing the sensitivity of protein detection. A field effect transistor (FET) for biomolecule sensing has shown high sensitivity, low cost implementation, and very short response times and is thus highly desired for implementing rapid immunoassays using portable systems.[11−13] However, complex automation is required to carry out sample pretreatment methods such as purification, dilution, and desalting while testing clinical samples, because of the Debye screening or charge screening effect in physiological salt environment.[14,15] The pressing demands of automation negatively impact the cost and convenience of FET-based protein assays, and sample

Received: January 20, 2019
Accepted: April 17, 2019
Published: April 17, 2019

DOI: 10.1021/acs.analchem.9b00353
Anal. Chem. 2019, 91, 5953−5960

processes such as dilution affect the immunogenic reactions, resulting in large variations.[16] More recently, organic transistors including electrochemical transistors and electrolyte-gated organic FETs have demonstrated very sensitive protein detection.[17,18] However, use of extra reagents like labels to affect redox reactions add to the complexity of the system, and stable mass production of organic FETs is not as mature as that of semiconductor-based counterparts.

In this work, we have developed an aptamer functionalized III−V semiconductor-based FET biosensor for the rapid and highly sensitive detection of NT-proBNP in clinical serum, without the requirement for additional sample preprocessing techniques. An AlGaN/GaN high electron mobility transistor (HEMT) is used for transduction, as it is highly sensitive, biocompatible (unlike Si), and thermally stable.[19,20] The unique sensing structure implemented in our HEMT biosensor facilitates protein detection in a high salt environment by overcoming the limitations of charge screening effects. An aptamer specific to NT-proBNP is used as the receptor, providing advantages such as stability, a longer shelf life, and ease of surface functionalization over traditional protein-based receptors. The sensing characteristics in physiological buffer and untreated human serum samples are demonstrated. The sensor demonstrates high sensitivity and selectivity, over the clinical range of detection of NT-proBNP, which indicates the potential applications in clinical diagnostics. Furthermore, we demonstrate a method to amplify and modulate the sensitivity of protein detection by means of varying sensor design. Higher sensitivity is obtained through the sensor design adopted in this work compared to that of traditional FET biosensors previously reported. This technology has a promising future in the in vitro diagnostics industry, particularly home-care diagnostics, owing to the short response time (5 min), low sample requirement (2.5−5 μL), and lack of extensive sample pretreatments.

EXPERIMENTAL SECTION

AlGaN/GaN HEMT Fabrication. The HEMT fabrication process begins with creating mesa structures on the epi-wafer, which is composed of a 3 μm thick undoped GaN layer and a 150 Å thick $Al_{0.25}Ga_{0.75}N$ layer on Si. The AlGaN/GaN is deposited by metal organic chemical vapor deposition (MOCVD). The device fabrication processes are described in Supplementary Figure S1. Inductively coupled plasma (ICP) etching is performed to create a device active area in the presence of Cl_2/BCl_3 gases at an ICP power of 300 W and RF bias of 120 W at 2 MHz. Then, ohmic metal contacts are deposited on the active area with the composition of Ti/Al/Ni/Au, with a thickness of 200/400/800/1000 Å, respectively, using an electron beam evaporator (E-beam). Following this, a two-step rapid thermal annealing (RTA) process is performed: the first step of annealing is carried out at 200 °C for 25 s and the second step at 850 °C for 40 s in an inert environment of N_2. The metal interconnections and the gate electrode (which is spaced apart from the channel), consisting of 200 Å of Ti and 1000 Å of Au, are deposited using an e-beam evaporator. The whole device is then passivated using a photoresist and using photolithography; the sensing region (i.e., the transistor channel and gate electrode) are selectively opened. The schematic illustration and real view of the device are shown in Figure 1. The miniaturized HEMT device can be embedded in a thermocurable polymer substrate, and using photolithography and an e-beam evaporator, metal interconnects can be laid, which can then be used for measurement and sensor readout with a portable biosensor system.[21]

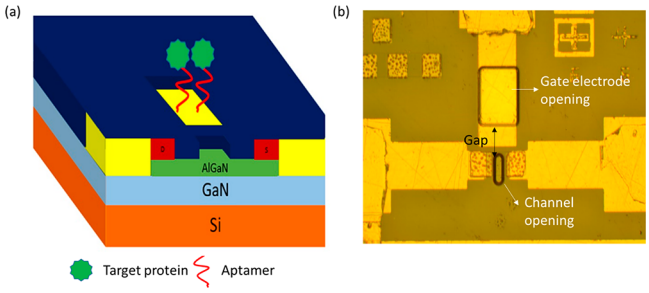

Figure 1. (a) Aptamer functionalized AlGaN/GaN HEMT biosensor. (b) Real view image of the HEMT chip showing the gate electrode and channel openings.

Aptamer Selection. The aptamer specific to NT-proBNP was screened and selected using Systematic Evolution of Ligands by Exponential Enrichment (SELEX), which was performed on an integrated microfluidic system.[22] Briefly, magnetic beads surface-coated with NT-proBNP were mixed with a single-stranded DNA (ssDNA) library (concentration = 1 M, Medclub Scientific Co., Ltd., Taiwan) such that the ssDNA with high affinity toward NT-proBNP could bind with the magnetic beads. A magnetic field was then applied to collect the ssDNA−magnetic bead complexes, following which unbound ssDNA was washed away. The high affinity, captured ssDNA was heated and released for subsequent nucleic acid amplification using polymerase chain reaction (PCR). After several repeated cycles, an aptamer sequence with high affinity toward NT-proBNP was screened and selected.[22] The dissociation constant (K_d) of the aptamer specific to NT-proBNP was measured to be 2.89 nM.

Surface Functionalization. The surface functionalization process is schematically described in Supplementary Figure S2. The NT-proBNP specific aptamer is thiolated at the 5-prime side. The thiolated aptamer and thiol reducing agent, Tris(2-carboxyethyl) phosphine (TCEP), are mixed in the molar ratio of 1:1000 in tris-ethylenediaminetetraacetic acid (EDTA) buffer (TE buffer). After incubation at room temperature for 15 min, the aptamer containing solution is heated to 95 °C and flash cooled and dropped on the sensor for incubation at room temperature for 24 h.

Protein Samples. In the present work, two protein sample solutions, in 1× PBS and untreated clinical serum have been used. Purified NT-proBNP protein obtained from Abcam (catalog #ab51403, United Kingdom) is diluted to different concentrations in 1× PBS that contains 4% bovine serum albumin (BSA) to simulate human blood serum. Clinical samples of human serum with NT-proBNP received from patients are collected as per the National Cheng-Kung University Hospital institutional review board (IRB. No. B-ER-104−116) and under the guidance of National Tsing Hua University (IRB. No. 10405HE014). The clinical samples are used for electrical measurements without performing any further processing.

Measurement of Sensor. The electrical characterization of the HEMT sensor is performed using an Agilent B1530/B1500A semiconductor parameter analyzer. The $I-V$ characteristics of the sensor are provided in the supplementary section in Figure S3. A DC bias of 2 V is applied as the drain voltage, and a short duration (100 μs on-time) pulse of 1.5 V is applied to the separated gate electrode as the gate voltage.

DOI: 10.1021/acs.analchem.9b00353
Anal. Chem. 2019, 91, 5953−5960

When test solution is placed on the sensor and as the gate pulse is turned on, the potential drops in the solution, thereby changing the channel conductivity.

Protein Elution. After testing every sample containing NT-proBNP, the sensor is repeatedly washed in DI water and then incubated at 40 °C in DI water to disrupt the aptamer−protein binding and thereby elute the bound and unbound proteins away from the sensor surface. The sensor is later thoroughly rinsed in 1× PBS, and the sensor baseline is verified using electrical measurements to confirm that the sensor has been regenerated.

RESULTS AND DISCUSSION

The device structure is depicted in Figure 1. The gold electrode is spaced apart from the transistor active area and functionalized with an aptamer specific to NT-proBNP (Figure 1(a)). The top view image (Figure 1(b)) depicts the sensing area, which is composed of the openings on the gate electrode ($100 \times 120\ \mu m^2$) and the FET active area or the channel ($10 \times 60\ \mu m^2$) and are spaced apart at a distance of 65 μm. The sample solution placed on the sensor covers the two open areas, simulating a liquid capacitor, with two conductive plates (the FET channel and gate electrode) sandwiching a dielectric medium (test solution). Our previous works have demonstrated the sensing mechanism in the separated gate FET structure.[23] Briefly, the gate electrode is connected to a voltage source that applies a short duration gate pulse V_g (100 μs; 1.5 V), which drops across the solution placed in the gap between the gate electrode and the transistor dielectric (AlGaN). By using pulsed gate bias operation, heat induced FET baseline shifting commonly observed in DC bias operation of FET sensors can be avoided. Moreover, the pulsed operation ensures that there are no redox currents generated, and hence, only capacitive effects are displayed. This is confirmed by monitoring the gate electrode leakage current, which quickly relaxes to zero after pulse application, indicating the lack of resistive response due to redox currents. Therefore, the V_g applied can be represented mathematically as

$$V_g = \Delta V_s + \Delta V_d \tag{1}$$

where V_s and V_d refer to the voltages that drop in the test liquid and the transistor dielectric, respectively.

The pulse application redistributes the electrical double layer (EDL) occurring at the solid/liquid interfaces (i.e, the interface between the sample solution and the gate electrode and transistor dielectric). The changes in the double layer at the gate electrode interface will be mirrored in the double layer at the transistor dielectric interface. This generates a capacitance across the solution, C_s, which controls the voltage drop in the transistor dielectric. This potential that drops in the dielectric (V_d) eventually varies the channel drain current as the two-dimensional electron gas (2-DEG) in the interface between AlGaN and GaN, which forms as the transistor channel is highly responsive to the changes in the surface potential. Therefore, the impedances in the sensing system, in the solution, and the transistor dielectric modulate the sensor output response. By assuming these impedances are in series combination, we can denote the potential that drops across the dielectric as

$$\Delta V_d = \frac{\frac{1}{j\omega C_d}}{\frac{1}{j\omega C_d} + \frac{1}{j\omega C_s}} \times V_g = \frac{C_s}{C_d + C_s} \times V_g \tag{2}$$

where C_d, C_s, and ω are capacitances across the dielectric and solution as well as the angular frequency, respectively.

This shows that changes to the solution capacitance will result in changes in the potential drop across the dielectric, leading to changes in drain current response. The solution capacitance can change under different scenarios: when the ionic strength of the test medium is varied, when the surface property is changed because of functionalization of the gate electrode, and when the electrostatic interaction is modified at the gate electrode EDL via receptor−ligand binding.

Protein Detection in Buffer: NT-proBNP Tested in 1× Phosphate Buffered Saline. The liquid-capacitor-like operation of the GaN HEMT biosensor facilitates direct protein detection in high ionic strength media. This is demonstrated by testing for NT-proBNP prepared in 1× PBS that contains 4% BSA. In the human plasma, albumin occurs as the most abundant protein, and 4% BSA is added to the buffer to simulate the physiological plasma proteome conditions. The purified NT-proBNP is diluted to desired test concentrations in albumin containing buffer (0.25, 0.5, 1, 2, 5, 10 ng/mL). Prior to testing the target proteins, the sensor baseline is measured with zero target concentration in the albumin containing buffer solution. The sample was placed on the sensor region with 5 min incubation at room temperature, after which electrical measurements were conducted. The drain current response for different NT-proBNP test concentrations in albumin containing buffer is shown in Figure 2(a). When

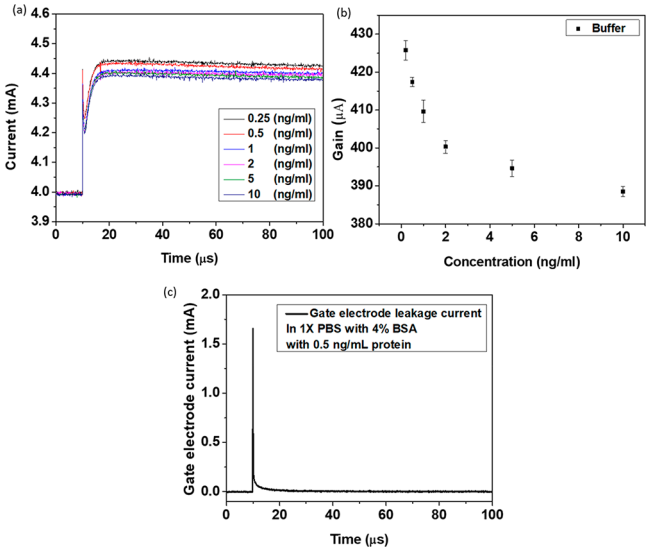

Figure 2. NT-proBNP detection in albumin containing buffer. (a) Drain current vs time graph. (b) Sensor calibration curve depicting current gain vs NT-proBNP concentration (n = 3). (c) Gate electrode leakage current depicting the absence of charge transfer reactions.

the concentration of NT-proBNP increases, the drain current reduces. This is due to the changes in the electrostatic interaction in the vicinity of the double layer at the electrode/solution interface, where the immobilized aptamer captures the target protein from the test solution. The intense electrostatic interaction of the aptamer and protein induces charge redistributions in the EDL, leading to changes in the

DOI: 10.1021/acs.analchem.9b00353
Anal. Chem. 2019, 91, 5953−5960

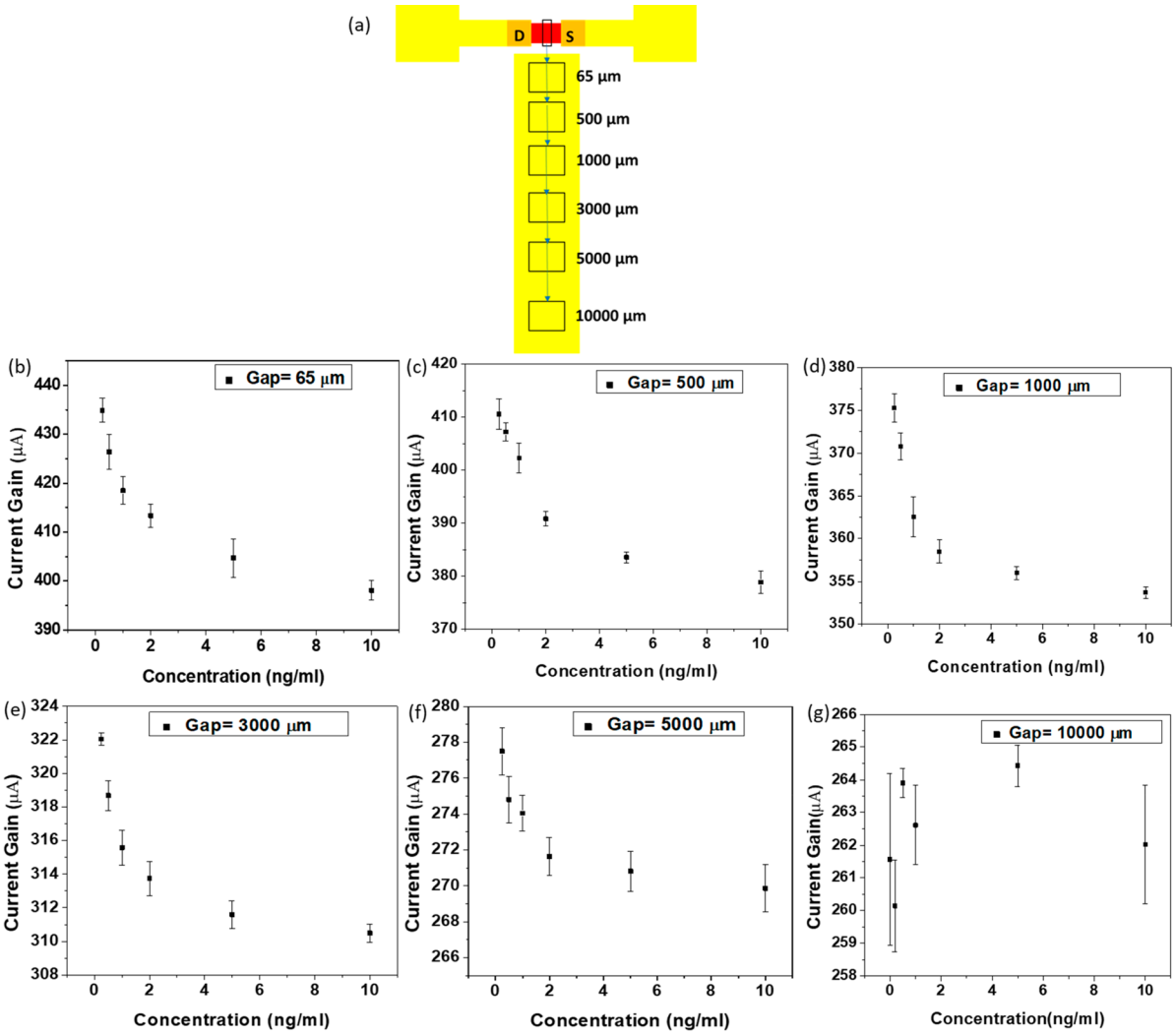

Figure 3. (a) Sensor with different spacings between channel and gate electrode. (b–g) NT-proBNP detection in albumin containing buffer in different gaps of 65, 500, 1000, 3000, 5000, and 10 000 μm, respectively (n = 3).

capacitance across the solution and hence the HEMT current response. In the present work, we utilize differential drain current as the sensor signal rather than the absolute drain current. The differential drain current hereon mentioned as the current gain or gain is defined as the difference in drain current response before and after V_g application (illustrated in Figure 2(a)). The current gain offers better stability, as the absolute drain current is prone to variations resulting from external sources and/or thermal effects. The sensor response curve can be obtained by plotting current gain versus NT-proBNP concentrations, as seen in Figure 2(b). The sensor shows elevated sensitivity across a vast dynamic range of detection from 0 to 10 ng/mL. Figure 2(c) shows the gate electrode leakage current (I_G) measured for our sensor. When the pulse is turned on, I_G peaks and then quickly relaxes to zero, which indicates that there are no charge transfer reactions. This eliminates the resistive component, and we can assume a purely capacitive model for our sensor response. In fact, the gate electrode leakage current is evidence that our sensor offers nonfaradaic response.

Tunable Sensitivity in Increased Ionic Strength. The main feature of our aptamer functionalized GaN HEMT biosensor is the ability to directly sense the target proteins in increased ionic strength environments without dilution or filtering. An FET sensor being a surface affinity type of sensor exhibits very high sensitivity as well. However, traditional FET biosensor design suffers from the drawbacks of charge screening effects, to overcome which deliberate test medium dilution has to be conducted. Using our unique sensor design, we have been able to detect proteins in 1× PBS, or in other words, we have been able to detect proteins beyond the Debye length. In this section, we will explore the phenomenon that facilitates the detection circumventing the charge screening effects and enhanced sensitivity in high salt concentration containing liquids. To illustrate the differences in transduction methodology of our GaN HEMT biosensor and traditional FET biosensors, we used different gap spacings between the gate electrode and transistor channel region. Different gaps in the sensing region were formed using photolithography that allowed the gate electrode opening to be positioned at 65, 500, 1000, 3000, 5000, and 10 000 μm from the transistor channel opening (Figure 3(a)). The sample solution is placed on the sensor, covering the gate electrode and channel openings. After 5 min of sample incubation, drain current response is recorded. The test results are shown in Figure 3, which depicts sensor response curves obtained for NT-proBNP detection in albumin containing buffer, for different gaps (from 65 to 10 000 μm). From the results in Figure 3(b–g), it can be seen

DOI: 10.1021/acs.analchem.9b00353
Anal. Chem. 2019, 91, 5953–5960

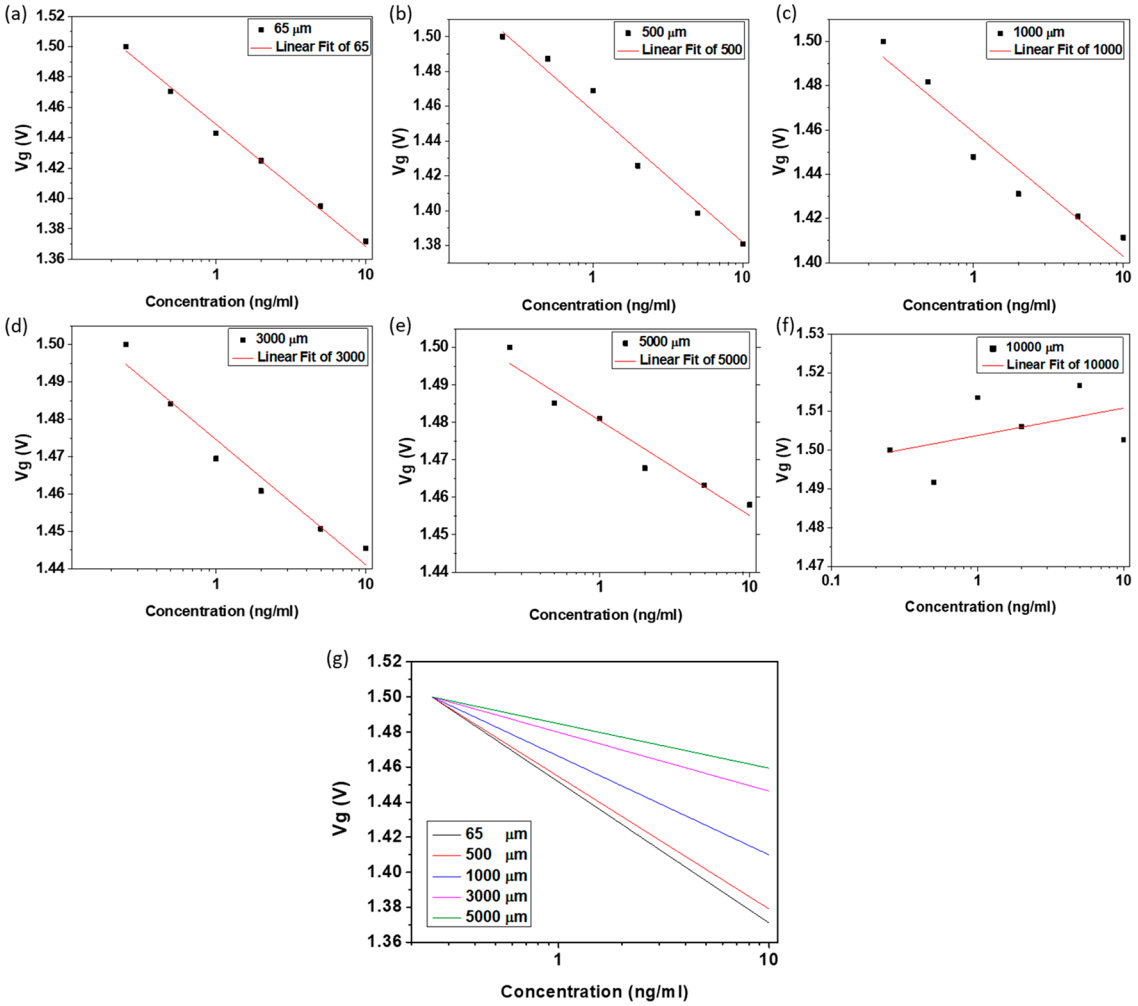

Figure 4. (a–f) V_g versus NT-proBNP concentration curves for different gaps of 65, 500, 1000, 3000, 5000, and 10 000 μm, respectively. (g) Consolidated V_g versus NT-proBNP concentration curves.

that a larger change in current gain corresponding to NT-proBNP test concentrations are observed for smaller gaps. This means that sensitivity is larger when the spacing between the gate electrode and the channel is smaller.

A quantitative comparison of sensitivity can be obtained by expressing the sensor signal in terms of the change in effective V_g because of protein binding with the aptamer. This is depicted in Figure 4 as V_g versus protein concentration plots. The method of extrapolation of effective V_g versus concentration is shown in detail in Supplementary Figure S4. Briefly, the current gain is expressed in terms of applied V_g, and when current gain versus concentration curves are obtained for different gap configurations (as in Figure 3), the y axis can be converted to represent effective V_g that corresponds to different NT-proBNP concentrations. The plots in Figure 4 are expressed in logarithmic scale to elucidate the linearity over a wide range of protein concentrations. Figure 4(a–f) correspond to V_g versus log concentration curves for sensing structures with gaps of 65, 500, 1000, 3000, 5000 and 10 000 μm, respectively. Linear fitting of the response curve is carried out to obtain the sensitivity, which is consolidated and depicted in Figure 4(g). The sensitivities obtained from response curves are 80.54, 75.54, 56.26, 33.53, and 25.38 mV/decade concentration at gaps of 65, 500, 1000, 3000, and 5000 μm, respectively. At a 10 000 μm gap, there is no protein detection as indicated by the minimal change in current gain (as in Figure 4(f)). Table 1 summarizes the sensitivity values obtained at different gaps and shows the quality of fitting used to obtain the sensitivity values. The results in Figure 4(g) demonstrate quantitatively that enhanced sensitivity can be obtained with smaller gaps between the gate electrode and the channel. The smaller gap in the sensing region leads to less potential drop in the solution, which effectively leads to a larger drain current gain. In the design of traditional FET biosensors, the reference electrode is either unbiased or given a very low bias and arbitrarily positioned extremely far away from the transistor active region.[24] This sensing structure is similar to our experimental design of the 10 000 μm gap, which generates a large potential drop in the sensing region, leading to a low drain current gain, with which it is difficult to distinguish different protein concentrations. In that scenario, the potential changes induced by receptor–ligand binding on

Table 1. Sensitivity Values Corresponding to Different Gaps between Channel and Electrode

gap	65 μm	500 μm	1000 μm	3000 μm	5000 μm
sensitivity	80.54 mV/decade	75.54 mV/decade	56.26 mV/decade	33.53 mV/decade	25.38 mV/decade
R-square	0.994	0.974	0.920	0.950	0.940

DOI: 10.1021/acs.analchem.9b00353
Anal. Chem. 2019, 91, 5953–5960

the active area is largely reduced in high salt concentrations because of the strong charge screening, which limits the detection of the surface potential changes.

Bergveld had developed a model for the MOSFET-based pH sensor based on Boltzmann distribution and electric double layer theory to predict the sensitivity, which is not larger than 59.2 mV/decade.[25,26] This predicted ideal sensitivity is exactly the same as the ideal sensitivity in the Nernst equation, which is frequently used in potentiometry.[25] This is very interesting, and a question arises. Is it possible to generate a sensitivity higher than the ideal sensitivity for ion-selective FET? Previously, our group has published lead- and mercury-ion-selective FET sensors, which exhibit sensitivity higher than the ideal Nernst sensitivity, based on our new methodology.[27,28] In this study, we would like to prove the enhanced sensitivity can also be achieved with FET-based protein sensors. Here, we have shown the enhancement in sensitivity, which can be as high as 80 mV/decade for protein detection, and it is significantly higher than the reported sensitivity in the range of 10−30 mV/decade.[29−33] Our sensor design thus offers a technique of tuning and amplifying the sensitivity for FET biosensors. The enhancement in sensitivity reported in this work has been quantitatively correlated with the sensor design (i.e., the gap between the gate electrode and FET active area (Figure 4)). In the future, more study in the theoretical model will be needed to explain the enhancement in sensitivity with a strong basis of physics. However, through this work, we are able to depict that by modulating the FET sensor design, we can indeed elevate the sensitivity of protein detection. Furthermore, we can obtain high sensitivity in a physiological salt environment without performing any pretreatments of the test sample. By tuning the gate voltage bias and the gap between the gate electrode and channel, we can enhance the sensitivity as desired by the application of the sensor.

Detection of NT-proBNP in Human Serum. The direct protein detection capabilities demonstrated in high salt containing solutions like 1× PBS can be further extended to real physiological fluids such as human serum. The human serum samples obtained from patients contain NT-proBNP. The concentration of NT-proBNP in serum samples is determined using standard clinical diagnostics. The NT-proBNP concentrations so determined used in our study are 0.2239, 0.5076, 1.1050, 2.7470, 4.6210, and 11.4970 ng/mL. The assay protocols for testing serum samples remain essentially the same. The serum sample was allowed to incubate on the sensor for 5 min before the measurement of electrical response. The test results are shown in Figure 5(a,b). Similar to the sensor response in 1× PBS with 4% BSA, the drain current decreases as the protein concentration increases. The sensor response curve (Figure 5(b)) reveals good NT-proBNP concentration dependency. This highlights an important feature of the GaN HEMT biosensor: selectivity toward the target protein. The aptamer is specific to NT-proBNP and captures the protein from the test solution during the sample incubation period. However, in human serum, there are various matrix proteins that occur in concentrations several orders higher in concentration than that of the target protein. During sample incubation, the background proteins may also exert weak forces on the aptamer and/or sensor surface, but they are nonspecific interactions and hence relatively much weaker than specific interactions. The strong electrostatic interaction between the aptamer and target protein will dominate during the short sample solution incubation duration

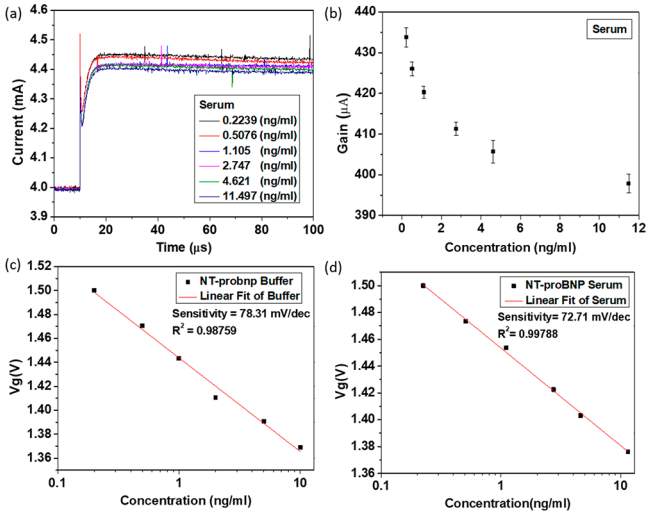

Figure 5. NT-proBNP detection in untreated human sera. (a) Drain current versus time graph. (b) Sensor calibration curve depicting current gain versus NT-proBNP concentration. (c,d) V_g versus concentration graphs for buffer and serum, respectively (n = 3).

of 5 min, leading to charge redistribution within the EDL and thus modulating solution capacitance and eventually the sensor current signal. The electrical test results in Figure 5 demonstrate that even in the existence of very high matrix protein concentration, the sensor is able to deliver good target protein concentration dependent on the drain current response. A comparison of sensitivity in buffer and serum is carried out in Figures 5(c,d). The gain versus concentration curves obtained by testing in albumin containing buffer and serum are converted to effective V_g versus log concentration curves. In this way, we can normalize the sensitivity obtained from different tests. In buffer, the sensitivity is 78.31 mV/decade, and in serum, it is 72.71 mV/decade NT-proBNP concentration. The sensitivity values are very similar, and this experimentally proves that in our sensing methodology, there is minimal interference of nonspecific binding in sensor signal, which contributes to high selectivity even in untreated clinical serum samples. As seen from Figure 4, by shortening the gap between the electrode and channel, thereby creating less potential drop across the sample solution under test, we can amplify the sensitivity and detect very low concentrations of target protein. The elevated sensitivity obtained under high electric field generation can facilitate the detection of proteins in increased ionic strength environments such as clinical serum, without any additional preprocessing of the test sample. This is indeed an important feature of our technology, which will greatly scale down the cost and complexity to obtain superior sensing characteristics required for point-of-care/home-care applications. The features of high sensitivity and selectivity exhibited by the aptamer functionalized HEMT biosensor are crucial in developing clinical applications for this technology.

To control the test background and reduce accumulation of nonspecific binding, the sensor chip is washed in DI water and 1× PBS, after testing each sample. The detailed washing procedure is described in the Experimental Section. The very low salt concentration in DI water is used to disrupt the receptor−ligand binding as well as other nonspecific interactions on the sensor surface. After washing with elution buffer, 1× PBS is used to restore the test background to native

DOI: 10.1021/acs.analchem.9b00353
Anal. Chem. 2019, 91, 5953−5960

conditions. In this way, the sensor baseline characteristics are restored to initial conditions prior to each protein sample test. The baseline regeneration results are depicted in Supplementary Figure S5. We can see that the sensor baseline can be restored between each test in albumin containing buffer and serum environments. This demonstrates that the decrease in current observed in the response curves in Figures 2 and 5 are indeed resultant from the specific aptamer−protein interactions and not from accumulation of nonspecific binding. The protein elution is an effective way to tightly control and maintain similar test background for assaying each protein sample.

CONCLUSION

In this study, we realized an aptamer functionalized AlGaN/GaN HEMT biosensor for detecting NT-proBNP from human serum, with amplified and tunable sensitivity. The sensor is operated under high electric field such that a liquid capacitor is generated at the sensing region, which modulates the FET channel conductivity with high sensitivity. Using the high field modulation technique, we can eliminate the charge screening effect in high salt environment, thus enabling direct detection of protein biomarkers in physiological fluids such as serum (untreated clinical samples). Because a highly selective aptamer is employed as opposed to a conventional protein-based receptor, we can obtain better stability and longer shelf life for the biosensor, making our sensor methodology highly desirable for in vitro diagnostics. We demonstrate the sensing and selectivity characteristics of the GaN HEMT biosensor using purified protein samples in albumin containing buffer and clinical serum samples. A detailed and systematic investigation of the enhanced sensitivity of our FET biosensor is carried out. It is revealed that by optimizing the sensor design (gap and applied potential), we can modulate the sensitivity. This technology can also be implemented for rapid, multiplexed cardiac marker detection in clinical samples and for CVD risk assessment and prevention.

ASSOCIATED CONTENT

Supporting Information

The Supporting Information is available free of charge on the ACS Publications website at DOI: 10.1021/acs.analchem.9b00353.

Additional schematics and experimental results (PDF)

AUTHOR INFORMATION

Corresponding Authors

*E-mail: ylwang@mx.nthu.edu.tw. (Y.-L.W.)
*E-mail: gwobin@pme.nthu.edu.tw. (G.-B.L.)

ORCID

Anirban Sinha: 0000-0002-4520-2859
Yu-Lin Wang: 0000-0002-4791-936X

Notes

The authors declare no competing financial interest.

ACKNOWLEDGMENTS

This work was partially supported by research grants from the Ministry of Science & Technology (MOST 107-2218-E-007-021, MOST 106-2218-E-007-015-MY2) and National Tsing Hua University (107Q2526E1, 107Q2713E1). We thank the technical support from National Nano Device Laboratories (NDL) in Hsinchu and the Center for Nanotechnology, Materials science, and Microsystems (CNMM) at National Tsing Hua University.

REFERENCES

(1) Song, Y.; Huang, Y.-Y.; Liu, X.; Zhang, X.; Ferrari, M.; Qin, L. *Trends Biotechnol.* **2014**, *32* (3), 132−139.
(2) Johnson, C. J.; Zhukovsky, N.; Cass, A. E. G.; Nagy, J. M. *Proteomics* **2008**, *8* (4), 715−730.
(3) Gilstrap, L. G.; Wang, T. J. *Clin. Chem.* **2012**, *58* (1), 72−82.
(4) van Holten, T. C.; Waanders, L. F.; de Groot, P. G.; Vissers, J.; Hoefer, I. E.; Pasterkamp, G.; Prins, M. W. J.; Roest, M. *PLoS One* **2013**, *8* (4), No. e62080.
(5) Dhingra, R.; Vasan, R. S. *Trends Cardiovasc. Med.* **2017**, *27* (2), 123−133.
(6) Lin, D. C. C.; Diamandis, E. P.; Januzzi, J. L.; Maisel, A.; Jaffe, A. S.; Clerico, A. *Clin. Chem.* **2014**, *60* (8), 1040−1046.
(7) Sharma, A.; Felker, G. M. *JACC: Heart Failure* **2016**, *4* (7), 548−550.
(8) Savarese, G.; Musella, F.; D'Amore, C.; Vassallo, E.; Losco, T.; Gambardella, F.; Cecere, M.; Petraglia, L.; Pagano, G.; Fimiani, L.; Rengo, G.; Leosco, D.; Trimarco, B.; Perrone-Filardi, P. *A Meta-Analysis* **2014**, *2* (2), 148−158.
(9) Taylor, C. J.; Roalfe, A. K.; Iles, R.; Hobbs, F. D. R. *BMJ. Open* **2014**, *4* (4), No. e004675.
(10) Kemperman, H.; van den Berg, M.; Kirkels, H.; de Jonge, N. *Clin. Chem.* **2004**, *50* (9), 1670−1672.
(11) Wang, C.; Cui, X.; Li, Y.; Li, H.; Huang, L.; Bi, J.; Luo, J.; Ma, L. Q.; Zhou, W.; Cao, Y.; Wang, B.; Miao, F. *Sci. Rep.* **2016**, *6*, 21711.
(12) Chen, J.-C.; Chou, J.-C.; Sun, T.-P.; Hsiung, S.-K. *Sens. Actuators, B* **2003**, *91* (1), 180−186.
(13) Fernández, D. G.; Blanco, A.; Durán, A.; Jiménez-Jorquera, C.; Fuentes, O. A.-d. *J. Phys.: Conf. Ser.* **2013**, *421* (1), 012015.
(14) Elnathan, R.; Kwiat, M.; Pevzner, A.; Engel, Y.; Burstein, L.; Khatchtourints, A.; Lichtenstein, A.; Kantaev, R.; Patolsky, F. *Nano Lett.* **2012**, *12* (10), 5245−5254.
(15) Stern, E.; Vacic, A.; Rajan, N. K.; Criscione, J. M.; Park, J.; Ilic, B. R.; Mooney, D. J.; Reed, M. A.; Fahmy, T. M. *Nat. Nanotechnol.* **2010**, *5* (2), 138−142.
(16) Reverberi, R.; Reverberi, L. *Blood Transfus.* **2007**, *5* (4), 227−240.
(17) Fu, Y.; Wang, N.; Yang, A.; Law, H. K.-w.; Li, L.; Yan, F. *Adv. Mater.* **2017**, *29* (41), 1703787.
(18) Wang, N.; Yang, A.; Fu, Y.; Li, Y.; Yan, F. *Acc. Chem. Res.* **2019**, *52* (2), 277−287.
(19) Lee, H. H.; Bae, M.; Jo, S.-H.; Shin, J.-K.; Son, D. H.; Won, C.-H.; Jeong, H.-M.; Lee, J.-H.; Kang, S.-W. *Sensors* **2015**, *15* (8), 18416−18426.
(20) Huang, C.-C.; Lee, G.-Y.; Chyi, J.-I.; Cheng, H.-T.; Hsu, C.-P.; Hsu, Y.-R.; Hsu, C.-H.; Huang, Y.-F.; Sun, Y.-C.; Chen, C.-C.; Li, S.-S.; Andrew Yeh, J.; Yao, D.-J.; Ren, F.; Wang, Y.-L. *Biosens. Bioelectron.* **2013**, *41*, 717−722.
(21) Hsu, C.-P.; Chen, P.-C.; Pulikkathodi, A. K.; Hsiao, Y.-H.; Chen, C.-C.; Wang, Y.-L. *ECS J. Solid State Sci. Technol.* **2017**, *6* (5), Q63−Q67.
(22) Sinha, A.; Gopinathan, P.; Chung, Y.-D.; Lin, H.-Y.; Li, K.-H.; Ma, H.-P.; Huang, P.-C.; Shiesh, S.-C.; Lee, G.-B. *Biosens. Bioelectron.* **2018**, *122*, 104−112.
(23) Chu, C.-H.; Sarangadharan, I.; Regmi, A.; Chen, Y.-W.; Hsu, C.-P.; Chang, W.-H.; Lee, G.-Y.; Chyi, J.-I.; Chen, C.-C.; Shiesh, S.-C.; Lee, G.-B.; Wang, Y.-L. *Sci. Rep.* **2017**, *7* (1), 5256.
(24) Kaisti, M. *Biosens. Bioelectron.* **2017**, *98*, 437−448.
(25) Bergveld, P. ISFET, Theory and Practice. Proceedings of the IEEE Sensor Conference Toronto, 2003, pp 1−26.
(26) Parizi, K. B.; Xu, X.; Pal, A.; Hu, X.; Wong, H. S. P. *Sci. Rep.* **2017**, *7*, 41305.
(27) Chen, Y.-T.; Sarangadharan, I.; Sukesan, R.; Hseih, C.-Y.; Lee, G.-Y.; Chyi, J.-I.; Wang, Y.-L. *Sci. Rep.* **2018**, *8* (1), 8300.

DOI: 10.1021/acs.analchem.9b00353
Anal. Chem. 2019, 91, 5953−5960

(28) Chen, Y.-T.; Hseih, C.-Y.; Sarangadharan, I.; Sukesan, R.; Lee, G.-Y.; Chyi, J.-I.; Wang, Y.-L. *ECS J. Solid State Sci. Technol.* **2018**, *7* (9), Q176−Q183.
(29) Cheng, S.; Hotani, K.; Hideshima, S.; Kuroiwa, S.; Nakanishi, T.; Hashimoto, M.; Mori, Y.; Osaka, T. *Materials* **2014**, *7* (4), 2490−2500.
(30) Lee, D.-W.; Lee, J.; Sohn, I. Y.; Kim, B.-Y.; Son, Y. M.; Bark, H.; Jung, J.; Choi, M.; Kim, T. H.; Lee, C.; Lee, N.-E. *Nano Res.* **2015**, *8* (7), 2340−2350.
(31) Hideshima, S.; Fujita, K.; Harada, Y.; Tsuna, M.; Seto, Y.; Sekiguchi, S.; Kuroiwa, S.; Nakanishi, T.; Osaka, T. *Sensing and Bio-Sensing Research* **2016**, *7*, 90−94.
(32) Münzer, A. M.; Seo, W.; Morgan, G. J.; Michael, Z. P.; Zhao, Y.; Melzer, K.; Scarpa, G.; Star, A. *J. Phys. Chem. C* **2014**, *118* (31), 17193−17199.
(33) Gao, N.; Gao, T.; Yang, X.; Dai, X.; Zhou, W.; Zhang, A.; Lieber, C. M. *Proc. Natl. Acad. Sci. U. S. A.* **2016**, *113* (51), 14633−14638.

DOI: 10.1021/acs.analchem.9b00353
Anal. Chem. 2019, 91, 5953−5960